**Proceedings of FEDSM'01**
**2001 ASME Fluids Engineering Division Summer Meeting**
**May 29- June 1, 2001-New Orleans, Louisiana**

# FEDSM2001-18133

# Development of a Loosely-Coupled Galerkin and Least Squares Finite Element Algorithm for Magnetoplasmadynamic Applications

**K.J. Berry[A] and Subrata Roy[B]**

**Mechanical Engineering Department**
**Kettering University, Flint, MI 48504**
[A] jberry@kettering.edu; [B] sroy@kettering.edu

## ABSTRACT
This paper presents a loosely-coupled algorithm which solves for electro-magnetic field variables using least squares method combined with an unequal order Galerkin weak statement that solves for fluid dynamic field variables. The combined loosely-coupled Galerkin Least Squares *(GLS)* algorithm is very stable, with excellent convergence properties, and is employed to enhance the theoretical understanding of self-induced magnetoplasmadynamic (MPD) thrusters.

## INTRODUCTION
Most problems arising in fluid dynamics, solid mechanics, heat transfer, electromagnetic and other mathematical physics can be recast in the form of first-order differential equations that are derived from their appropriate conservation and constitutive laws, Eason, [1]. Eason provides the foundation for the method as it applies to general partial differential equations. The application of the least-squares methods for numerical solution of ellipitic boundary-value problems was initiated by Bramble and Schatz [2,3], with additional work by Varga [4], employing a finite-dimensional space of approximating functions similar to finite element methods.

When compared to the classical Galerkin weak statement (GWS), LS generally results in a reduction of order for the continuity requirement at the expense of introducing more unknowns. The subject least-squares finite element method (LSFEM) [5,6] is based on the requirement that the sum of the squares of the residuals of these differential equations and boundary conditions should be a minimum at the correct solution. This reduction is achieved by transforming the original differential equations into an equivalent system of first-order differential equations and leads to more stringent continuity requirements for the trial functions. Hence, the smoothness requirement for the space of approximate functions would be reduced, and $C^0$ elements would be applicable.

A theoretical analysis of LSFEM for elliptic systems of the Petrovsky type was developed by Wendland [7], and the optimal error estimates were obtained. Petrovsky systems are an important sub-class of elliptic systems in which the equations and the unknowns have the same 'differentiability order'. An LSFEM formulation for inviscid Euler equations was proposed by Fletcher [8]. Jiang and Chai [9], applied LSFEM to a first-order quasi-linear system for compressible potential flow. Nguyen and Reyen [10] presented a space-time LSFEM for the advection-diffusion problems. Their numerical results show that the use of upwinding techniques for the Taylor-Galerkin approach turns out to be unnecessary when the least-squares weak formulation is extended into the time domain using standard shape functions.

An error estimate for the LSFEM solution of Cauchy-Rieman type equations was given by Fix and Rose [11]. Jiang and Povinelli [12] emphasize the universality of LSFEM, the symmetry and positiveness of the algebraic systems, the accommodation of LSFEM to equal-order interpolations for incompressible flows, and the numerical dissipation of LSFEM for convective transport problems and high-speed compressible flows. Tang and Tsang [15] used the LSFEM to investigate the phenomenon of natural convection caused by temperature and concentration buoyancy effects in rectangular enclosures. In addition to being stable, the method did not require a good initial guess as most steady-state solutions algorithms.

The use of preconditioned conjugate gradient (PCG) iterative solvers with the LSFEM was investigated by Jiang et al. [16-17] for 2D and for 3D-cavity flow. Due to the systems of equations that are always symmetric and positive-definite, results in opportunities to employ robust matrix-free conjugate gradient methods. PCG iterative solves were also used by Tang and Tsang [18,19]. The implementation of the LSFEM for first-order electromagnetic systems, combined with the application of GWS for higher-order fluid dynamics systems, is first introduced by Berry and Roy [20].

As a complement to [20], this paper describes the theoretical and numerical development for the *loosely-coupled* GLS. In the following sections the algorithm details are presented along with convergence and simulation results for MPD thrusters.

## NOMENCLATURE
$b_l$ – Local Magnetic Field (Weber/m$^2$)
B – Magnetic Field (Weber/m$^2$)
E – Electric Field (V/m)

h – Enthalpy (J/kg)
J– Current Density ($A/m^2$)
k – Thermal Conductivity (W/m-K)
p – Pressure (Pa)
R – Gas Constant (J/kg-K)
T – Temperature (K)
V – Velocity (m)
$\rho$ - Density ($kg/m^3$)
$\mu_f$ - Fluid Viscosity (Pa-s)
$\mu_0$ - Permeability of Free Space (W/A-m)
$E_c$ - Electron Charge (c)
$I_m$ - Ion Mass (kg)
H - Hall Parameter ($b_l \sigma/P_n E_c$)
$P_n$ – Plasma Number Density ($\rho/I_m$- Particles/$m^3$)
$\sigma$ - Electrical Conductivity (mho/m)
$\phi$ - Voltage (V)
$\gamma$ - Specific Heat Ratio
$T_e$ – Exit Thrust (N)
$V_e$ – Exit Velocity (m/s)

Subscripts

0 – reference value
t – tank condition
e – exit condition
*el* – element

The LSFEM discussed herein requires the minimization of the differential equation residual in the $L_2$ norm, where $L_2(\Omega)$ denotes the space of square-integrable functions. For a general state vector {u}, where $u_i = u(x_i)$ and $u_j = u(x_j)$, we define on $\Omega$ the inner product as:

$$(u_i, u_j) = \int_\Omega u_i u_j \, d\Omega, \quad u_i, u_j \in L_2(\Omega), \text{ with norm:}$$

$$\|u\|_0^2 = (u_i, u_i), \quad u_i \in L_2(\Omega)$$

Consider the following boundary value problem (BVP):

$$\begin{aligned} Lu - f &= 0 \quad in\ \Omega \\ Bu - g &= 0 \quad on\ \Gamma, \end{aligned} \tag{1}$$

where *f* is a given vector-valued function, *B* is a boundary operator, *g* is a given vector-valued function on the boundary that is assumed to be zero, and L is a linear first-order partial differential operator,

In (1), $\Omega \in R^n$ is a bounded domain with a piecewise smooth boundary $\Gamma$, and n=2,3 represents spatial dimensions. Considering the boundary condition of the BVP and defining an appropriate Sobolev function space, S, the minimization of the residual with respect to unknown vector *u*, leads to the least-squares weak statement [7]:

$$(Lw, Lu) = (Lw, f) \quad \forall w \in S \tag{2}$$

where $\delta u = w$ and $u \in S$.

**FINITE ELEMENT DISCRETIZATION**

We first discretize the computational domain as a union of finite elements and then introduce an appropriate basis function. Let *'ne'* denote the number of element nodes, *'m'* denote the degrees-of-freedom per node, *{u}* denote a vector containing '*M*' nodal parameter values (M = ne x m), and *{N(x)}* denote the element basis or shape function vector. If equal-order interpolation is assumed for all unknown element variables, we can write the expansion:

$$U(x_i) = \{N(x_i)\}^T \{u\} \tag{3}$$

where $U(x_i)$ is the value of unknown state vector {u} at location $x_i$. Introducing (3) into the least-squares weak statement (2) results in linear equation system of the form:

$$[K_{el}]\{U\} = \{F\}$$

where {U} is the global vector of nodal values. The global matrix [K] is assembled from the element matrices:

$$\begin{aligned} [K_{el}]_b &= \sum_{i=1}^{ne} \sum_{j=1}^{ne} [k(i,j)]_m \\ &= \int_{\Omega_e} \left[L(N_i(x))\right]^T \left[L(N_j(x))\right] \left\{U^{n+1}\right\} d\Omega \end{aligned} \tag{4}$$

where $[K_{el}]$ is a square matrix of size *(b=ne x m)* and [k(i,j)] is a square sub-matrix of size *m* in which $\Omega_e \subset \Omega$ is the domain of the *eth* element. The body force/residual vector {F} is assembled from the element vectors:

$$\{F_e\} = \int_{\Omega_e} \left[L(N_i(x))\right]^T \left\{ f_e + \frac{A_0}{\Delta t} U^n \right\} d\Omega$$

in which from (1):

$$\begin{aligned} \left[L(N_i(x))\right] &= \frac{A_0}{\Delta t} N_i(x) + [A] N_i(x) \\ &\quad + \sum_{i=1}^{nd} [A_i] \frac{\partial N_i(x)}{\partial x_i} \end{aligned} \tag{5}$$

where $\Delta t = t^{n+1} - t^n$ and *n* denotes the nth time level. The matrix [K] is always symmetric and positive definite (SPD) and thus, iterative robust solution methods may be employed. It is also important to emphasize that there are no weighting or upwind parameters, nor is there any added dissipation, or other non-physical ad-hoc modifications to the system of equations. The LSFEM solves the primary unknown variables in a fully-coupled manner, no splitting or projection (which may lead to convergence difficulties) is involved. Besides the finite element interpolation and the linearization, no other approximation is introduced. Therefore, the method is accurate and robust. In addition, LSFEM allows for the

possibility of more system equations than unknown variables, which is a major advantage for electromagnetic applications.

**LEAST SQUARES MHD**

To obtain a better understanding of parameters affecting the behavior of MHD (Electromagnetics and Fluid Dynamics) related problems, we derive a set of dimensionless equations using the following variables:

$$V^* = \frac{V}{V_0}, \qquad T^* = \frac{T}{T_0}, \qquad P^* = \frac{P - P_t}{P_0}$$
$$m_f{}^* = \frac{m_f}{m_{f0}}, \quad k^* = \frac{k}{k_0}, \qquad r^* = \frac{r}{r_0}$$
$$J^* = \frac{J}{J_0}, \quad B^* = \frac{B}{B_0}, \qquad E^* = \frac{E}{E_0}$$
$$h^* = \frac{h}{h_0}, \qquad r^* = \frac{r}{X_0}, \qquad \nabla^* = X_0 \bullet \nabla$$

All other dimensionless and reference parameters are defined in Appendix A.

The basic MHD equations are the Maxwell's equations that govern the electromagnetics [21] and the Navier-Stokes equations that govern the fluid hydrodynamics [22]. These equations form the basis of MHD for a moving media and are coupled through viscous and magnetic forces that may be temperature dependent.

The steady state non-dimensional Maxwell equations are expressed as:

$$\begin{aligned} \nabla^* \bullet \vec{B}^* &= 0 \\ \nabla^* \times \vec{B}^* &= \vec{J}^* \\ \nabla^* \bullet \vec{J}^* &= 0 \\ \nabla^* \times \vec{E}^* &= 0 \end{aligned} \tag{6}$$

The necessary constitutive relation is Ohm's law expressed as:

$$\vec{J}^* = s^*(T^*)\left[\left(\frac{s_0 E_0}{J_0}\right)\vec{E}^* + \left(\frac{s_0 V_0 B_0}{J_0}\right)\vec{V}^* \times \vec{B}^*\right] \tag{7}$$

In (7), Ohm's law relates the current density $\vec{J}$ to the medium velocity $\vec{V}$, the electric field $\vec{E}$, and the magnetic field $\vec{B}$.

***Two-dimensional Axis-symmetric Electromagnetics***

Two-dimensional electromagnetics assume motion in the r-z plane and an induced magnetic field in the azimuthal direction only. The cylindrical electromagnetic field equations for $\{J_z, J_r, B_q, f\}$ are expressed in scalar form and dropping the "*" notation as:

$$\begin{aligned} &J_z - s(T)\left(-K_1\frac{\partial f}{\partial z} + K_2 v_r B_q\right) = 0 \\ &J_r - s(T)\left(-K_1\frac{\partial f}{\partial r} - K_2 v_z B_q\right) = 0 \\ &-B_q\frac{K_2}{K_1}\left(\frac{\partial v_z}{\partial z} + \frac{\partial v_r}{\partial r}\right) - \frac{J_r}{K_1}\frac{\partial}{\partial z}\left(\frac{1}{s(T)}\right) + \frac{J_z}{K_1}\frac{\partial}{\partial r}\left(\frac{1}{s(T)}\right) + \frac{1}{K_1 s(T)}\left(\frac{\partial J_r}{\partial z} - \frac{\partial J_z}{\partial r}\right) \\ &-\frac{K_2}{K_1}\left(v_z\frac{\partial B_q}{\partial z} + v_r\frac{\partial B_q}{\partial r}\right) = 0 \\ &\frac{\partial J_z}{\partial z} + \frac{\partial J_r}{\partial r} = 0 \end{aligned} \tag{8}$$

where:

$$K_1 = \frac{s_0 E_0}{J_0}$$
$$K_2 = \frac{s_0 V_0 B_0}{J_0}$$

In the above we imposed $\nabla \times \vec{E} = 0$ (which implies that $\vec{E} \equiv -\nabla f$, where $f$ is a scalar potential, i.e. Voltage). Equation (8) is of first order and appears to be well posed with four equations and four unknowns. However, the current densities and the induced magnetic field must be also satisfy:

$$\begin{aligned} J_z - \left(\frac{1}{r}\frac{\partial(rB_q)}{\partial r}\right) &= 0 \\ J_r + \frac{\partial B_q}{\partial z} &= 0 \end{aligned} \tag{9}$$

As such we have six equations and four unknowns that provides another degree of complexity. However, the LSFEM has no difficulty handling more equations than unknowns.

***Least Square Electromagnetics Formulation***

With reference to (5) the LSFEM [A] matrices (Appendix B) are evaluated for each node "i" to form the operator [L] and assembled to evaluate the element stiffness matrix using equation (4). To assist the reader, the horizontal labels represent the nodal degrees of freedom while the vertical labels represent the number of nodal system equations.

***Two-dimensional Axis-symmetric Fluid Dynamics***

The equations for the conservation of momentum and mass for steady compressible MHD flow are expressed in dimensionless vector notation as:

$$\begin{aligned} r(T)\left(\vec{V} \bullet \nabla\right)\vec{V} &= -\nabla p - \left[\nabla \bar{\bar{t}}\right] \\ &\quad - \frac{2}{3\,\mathrm{Re}}\nabla\left[m(T)\nabla \bullet \vec{V}\right] \\ &\quad + \Delta_0\, \vec{J} \times \vec{B} \\ \nabla \bullet \left(r\vec{V}\right) &= r\,\nabla \bullet \vec{V} + \vec{V}\,\nabla \bullet r = 0 \end{aligned} \tag{10}$$

where the stress tensor $\bar{t}$ is expressed as:

$$\bar{t} = -\frac{m(T)}{\mathrm{Re}}\left(\nabla\vec{V} + \nabla^T\vec{V}\right) \tag{11}$$

The term $\vec{J}\times\vec{B}$ in (10) represents the electromagnetic body force caused by the interaction of the applied current $\vec{J}$ and the induced magnetic field $\vec{B}$. Similarly, the conservation of energy may be expressed as:

$$\begin{aligned}\nabla\bullet\left(r\,h\vec{V}\right) = &-\nabla\bullet\vec{q} - \Phi_0\left(\bar{t}:\nabla\vec{V}\right)\\ &+\Pi_0\left(\vec{V}\bullet\nabla\right)p\\ &+\Psi_0\vec{E}\bullet\vec{J}\end{aligned} \tag{12}$$

where $\vec{E}\bullet\vec{J}$ represents the Joulean dissipation body force from the interaction of the applied electric field $\vec{E}$ and the applied current field $\vec{J}$.

The appropriate Fourier constitutive law and ideal gas closure relations are:

$$\begin{aligned}\vec{q} &= -\frac{k(T)}{Pe}\nabla T\\ r &= \frac{g\,Ma^2}{T}\left(\frac{P_t}{P_0} + P\right)\end{aligned} \tag{13}$$

where *Pe* is the Peclect number and *Ma* is the Mach number.

***Galerkin Finite Element Method (GFEM)***

With the unequal velocity-pressure formulation, we assume that the velocity components are interpolated at 'r' nodes, while the pressure is interpolated at 's' nodes, where in general r > s. This representation is required to remove any spurious pressure fields and is similar to the staggered grid approach employed in the finite difference method.

The finite element matrices are developed via Bubnov-Galerkin's weighted residual method. We require that a weighted value of a residual, *R*, be a minimum over the domain, $\Omega$, by employing piece-wise continuous interpolation functions, *N*. With Galerkin's method the weighting or interpolation functions are defined as the element shape functions, $N_i$. Thus, for each element node, i, we have:

$$\iiint_{\Omega} RN_i\,d\Omega = 0\ (i = 1,2,,,n)$$

where for cylindrical coordinate the differential volume is defined as $d\Omega = 2p\,rdrdz$.

Using Galerkin's method along with Green's theorem for integration by parts in 2D, the element matrices always result in a set of non-linear simultaneous equations [4] of the form:

$$[\mathbf{K}]\{U\} = \{F\}$$

where $\{U\} = \{v_z, v_r, T, r, p\}$ is the global solution vector, $\{F\}$ is the global force vector and [K] is the global stiffness matrix expressed as:

$$[K] = \begin{bmatrix} [K_{11}] & [K_{12}] & [K_{13}] & [K_{14}] & [K_{15}]\\ [K_{12}^T] & [K_{22}] & [K_{23}] & [K_{24}] & [K_{25}]\\ [K_{31}] & [K_{32}] & [K_{33}] & [K_{34}] & [K_{35}]\\ [K_{41}] & [K_{42}] & [K_{43}] & [K_{44}] & [K_{45}]\\ [K_{15}^T] & [K_{25}^T] & [K_{53}] & [K_{54}] & [0] \end{bmatrix}$$

The exact form of the global sub-matrices, $[K_{ij}]$, is provided in [20].

***Loosely-Coupled GLS Algorithm***

The loosely-coupled GLS algorithm is described as follows:

1. Initialize variables.
2. Compute currents, voltages and magnetic fields via LSFEM.
3. Update momentum loads.
4. Compute velocity, temperature, density, and pressure via GFEM.
5. Update thermal properties.
6. If not converged goto 2.
7. Post-process efficiency.
8. Stop.

The algorithm as described is efficient and very robust due to coupling of magnetic and flow variables using a direct wave front solver [23].

**MPD THRUSTER SIMULATION**

The *magnetoplasmadynamic (MPD)* thruster is being considered as a high power in-space propulsion system to support missions of interest to the NASA Earth Science, Space Science, and Human Exploration and Development of Space Strategic Enterprises. In this robust electric propulsion device arc current is utilized as an ionizer for the gaseous propellant that interacts with the self-induced magnetic field to accelerate the plasma, and produce the required thrust through an inherently unsteady process [24-26]. The MHD equations as presented above (1)-(5) can be used for MPD thruster analysis assuming a single fluid/ single temperature approximation. This implies the plasma to be fully and singly ionized. We also assume the plasma is described by a perfect gas equation of state.

In this section, we document the numerical simulation of an annular self-field thruster. Figure 1 shows a detailed schematic of the axis-symmetric thruster geometry showing dimensions, nodal locations, and region generation scheme. The model employed 8,576 biquadratic elements with

velocity, temperature, density, current, magnetic field, and voltage computed at all nine nodes of the element while pressure solution is computed at corner nodes only.

Argon gas propellant enters at temperature $T_0$, pressure, $P$, mass flow rate $\dot{m}$, and is ionized (within a few millimeters) caused by the applied current density, $J_0$. Therefore, in this model, the inlet temperature is chosen high enough such that the propellant is sufficiently ionized. As such, the upstream computational boundary is in reality a few millimeters downstream of the true gas entry through the backplate.

***Geometry and Boundary Conditions***

The MPD velocity boundary conditions assume a uniform inlet velocity, zero velocity along the fixed boundaries and a zero pressure gradient condition imposed at the downstream exit and along the upper downstream radial boundary. The thermal boundary condition assume an isothermal condition for the inlet and the anode, with a zero temperature gradient boundary condition imposed for all other surfaces. This represents an upper bound for thruster operation The electromagnetic boundary condition assume the anode and cathode have a constant potential difference, the entry back-plate is electrically insulated, zero downstream axial magnetic field values, and magnetic fields are constant at the computational boundary downstream. Although there are other boundary condition combinations, these appear to be ones that are logical and provide physically realistic results.

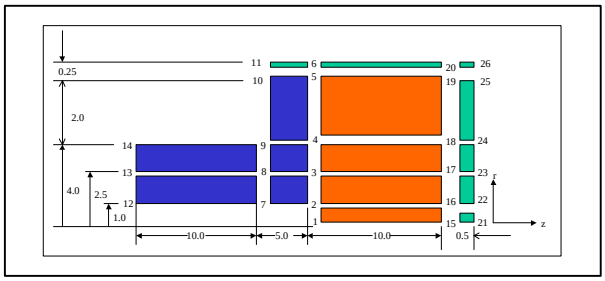


Figure 1. Geometric Model

From Figure 1 the following geometric variables are defined as:

Electrode Length ($L_e$): 10.0 cm

Inner Radius ($R_1$): 1.0 cm

Outer Radius ($R_2$): 4.0 cm

*Plasma Properties*

The propellant is Argon gas with the following specified operating conditions and property values:

Specific Heat Ratio ($g$): 1.667

Constant Pressure Specific Heat ($c_p$): 522 J/kg-K

Prandtl Number ($p_r$): 0.670

Inlet Temperature ($T_0$): 5,000K

Inlet Pressure ($P_t$): 1000 Pa

Gas Constant ($R_{gas}$): 208 J/kg-K

Other property values are determined from [27].

**MPD THRUSTER SIMULATION RESULTS**

An overall schematic for the MPD algorithm is provided in [20]. The algorithm employs 9-node quadrilateral finite elements with the following modeling parameters:

*Elements*: 8,576 9-node Quadrilateral Elements
*Nodes*: 34,412
*DOF*: 147,849$\{v_z, v_r, T, r, P\}$
137,648$\{J_z, J_r, B_q, f\}$
*Wave Front*: 895

The convergence parameter is defined as the *Residual Norm* expressed as: $\bar{R} = \dfrac{\sum_0^n \left|\left(Y^{m+1} - Y^m\right)\right|}{\sum_0^n \left|Y^m\right|} \le 10^{-5}$

where Y is the individual nodal degree of freedom, 'm' is the iteration index, and where the sum is over all nodal degrees of freedom.

Figures 2 and 3 show the fluid dynamics and electromagnetics equations convergence history, respectively, for a mass flow rate of 2 gm/s and a current of 4,000 amps. Note the rather stable computational behavior of the both the GFEM and the LSFEM algorithms.

Additional sample results are provided in Figures 4-7 that show contour plots for Speed, Temperature, Density, and Voltage, respectively. Results are shown for a mass flow rate of 2.25 gm/s and a current of 4,000 amps. Note the temperature increase along the insulated cathode surface and the velocity increase within a narrow region above the cathode surface. This velocity increase corresponds to the location of the maximum induced magnetic field (i.e. along the cathode surface). Also note the velocity decrease in the plasma core downstream of the inlet due to mass conservation. Observe the exit velocity increase due to heat transfer from the cathode to the anode. This heat transfer provides increased density and a corresponding increased convective fluid acceleration. Finally, the increased density creates density gradients that provide additional axial and radial momentum thrust forces.

Although not shown, the induced magnetic field has a maximum value along the cathode surface associated with a maximum radial current density. The larger cathode temperature and the associated temperature dependent electrical conductivity result in this maximum radial current density.

**CONCLUSIONS**

This paper presents a loosely-coupled single-fluid and single temperature MHD algorithm that combines the traditional Galerkin Finite Element Method and the Least Square Finite Element Method. The algorithm has good convergence properties, is very stable for typical MPD

operating conditions, and is applicable for steady compressible Magnetohydrodynamics fluid flow with heat transfer, assuming a fully ionized plasma.

Additionally, the Least Square Finite Element Method provides a framework for a unified approach applicable to interdisciplinary problems in fluid dynamics. This method is based upon a first-order differential equation formulation. Using $C^0$ finite elements to discretize the equations and minimize the $L_2$ norm of the residuals leads to a symmetric and positive-definite algebraic system that can be effectively solved by simple yet robust matrix-free iterative methods. Furthermore, using an Element-by-Element (EBE) Preconditioned Conjugate Gradient (PCG) approach will allow algorithm development that does not require the assembly of the global or local elemental stiffness matrices. This characteristic can effectively be utilized for the solution of large-scale problems on parallel computers.

Modeling improvements for increased accuracy are:

- An Equation of State (EOS) for real fluids
- Accurate Plasma Properties
- Transient Simulations
- Temperature dependent specific heats
- Inclusion of a two component model for ions and electrons
- Radiation effects

We anticipate these modeling improvements will be very useful when combined with geometry optimization algorithms to study thruster geometry affects on efficiency.

**REFERENCES**


1. E.D. Eason, A Review of Least-Squares Methods for Solving Partial Differential Equations, Int. J. Num. Methods Engrg., 10 (1976) 1021-1046.
2. J.H. Bramble and A. H. Shatz, On the Numerical Solution of Elliptic Boundary-Value Problems by Least-Squares Approximation of the Data, "Numerical Solution of PDE.," Vol. 2, Academic Press, New York (1970), 107-133.
3. J.H. Bramble and A. H. Shatz, Rayleigh-Ritz-Galerkin Methods for Dirichlet's Problems Using Subspaces Without Boundary Conditions, Comm Pure Appl. Math, 23 (1970), 653-675.
4. R.S. Varga, Function Analysis and Approximation Theory in Analysis, Regional Conference Series in Applied Mathematics, No. 3, SIAM, 1971.
5. P.P. Lynn and S.K. Arya, Use of the Least-Squares Criterion in the Finite Element Formulation, Int. J. Num. Methods Engrg., 6 (1973), 75-88.
6. O.C. Zienkiewicz, D.R.J. Owen and K.N. Lee, Least Squares Finite Element for Elastostatic Problems-Use of Reduced Integration, Int. J. Num. Numer. Methods Engrg. (1974), 341-358.
7. W.L. Wendland, Elliptic Systems in the Plane (Pitman, London, 1979)
8. C.A.J. Fletcher, A Primitive Variable Finite Element Formulation for Inviscid Compressible Flow, J. Comp. Phys. 33 (1979), 301-312.
9. B.N. Jiang and J.Z. Chai, Least Squares Finite Element Analysis of Steady High Subsonic Plane Potential Flows, Acta. Mech. Sinica (1980), 90-93.
10. H. Nguyen and J. Reynen, A Space-time Least-Squares Finite Element Scheme for Advection-Diffusion Equations, Comp. Methods Appl, Mech. Engrg, 42 (1984), 331-342.
11. G.J. Fix and M.E. Rose, A Comparative study of Finite Element and Finite Difference Methods for Cauchy-Rieman Type Equations, SIAM J. Numer. Anal, 22 (1985), 250-260.
12. Bo-Nan Jiang and L.A. Povinelli, Least_Squares Finite Element Method for Fluid Dynamics, Comp. Methods Applied Mechanics and Engrg, 81 (1990), 13-37.
13. Bo-Nan Jiang, A Least-Squares Finite Element Method for Incompressible Navier-Stokes Problems, Int. J. Num. Methods in Fluids, 14 (1992), 843-859.
14. L.Q. Tang and T.T.H. Tsang, A Least-Square Finite Element Method fr Time-dependent Incompressible Flows with thermal Convection, Int. J. Num. Methods in Fluids, 17 (1993), 271-289.
15. L.Q. Tang and T.T.H. Tsang, A Least-Squares Finite Element Method for Doubly-Diffusive Convection, Comp. Fluid Dyn., 3 (1994), 1-17.
16. Bo-Nan Jiang, T.L. Lin, and L.A. Povinelli, Large-Scale Computation of Incompressible Viscous Flow by Least-Squares Finite Element Method, Comput. Methods Appl. Mech. Engrg, 114 (1994), 213-231.
17. B.-N. Jiang and L.-J. Hou et al., Least-Squares Finite Element Solutions for Three-Dimensional Backward-Facing Step Flow, Comp. Fluid Dyn., 4 (1995), 1-19.
18. L.Q. Tang and T.T.H. Tsang, An Efficient Least-Squares Finite Element Method for Incompressible Flows and Transport Processes, Comp. Fluid Dyn., 4 (1995), 21-39.
19. L.Q. Tang and T.T.H. Tsang, Transient Solutions by a Least-Squares Finite-Element Method and Jocob Conjugate Gradient Technique, Numerical Head Transfer, 28 (1995), 183-198.
20. K.J. Berry, and S. Roy, Least Square FE Based MPD Algorithm for Practical Magnetoplasma Applications, AIAA 39th Aerospace Sciences Meeting, AIAA-2001-0200, Jan. 2001.
21. F.M. White, *Viscous Fluid Flow*, McGraw Hill, 1974.
22. W.F. Hughes and F.J. Young, *The Electromagnetodynamics of Fluids*, John Wiley, 1966.
23. K. J. Berry, An Efficient C Based Wave Front Solver for PC Finite Element Applications, Journal of Mechanical Engineering Systems, Vol. 1, No. 3, 1990.
24. F.F. Chen, Plasma Physics and Controlled Fusion, Plenum Press, 1984.
25. D.E. Hastings and E.H. Niewood, "Theory of the modified two-stream instability in a magnetoplasma-dynamic thruster," Journal of Propulsion and Power, Vol. 7, No. 2, pp. 258-268, 1991.
26. E.Y. Choueiri, *Electron-ion Streaming Instabilities of an Electromagnetically Accelerated Plasma*, PhD dissertation, Princeton University, 1991.
27. M. Lapointe, "Numerical simulation of self-field MPD thrusters," AIAA Paper No. 91-2341, 1991.

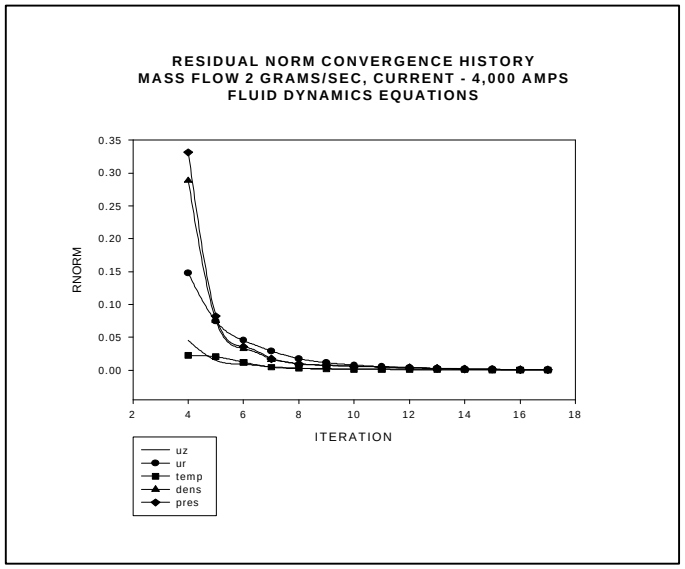


Figure 2. Residual Norm Convergence History – Fluid Dynamics

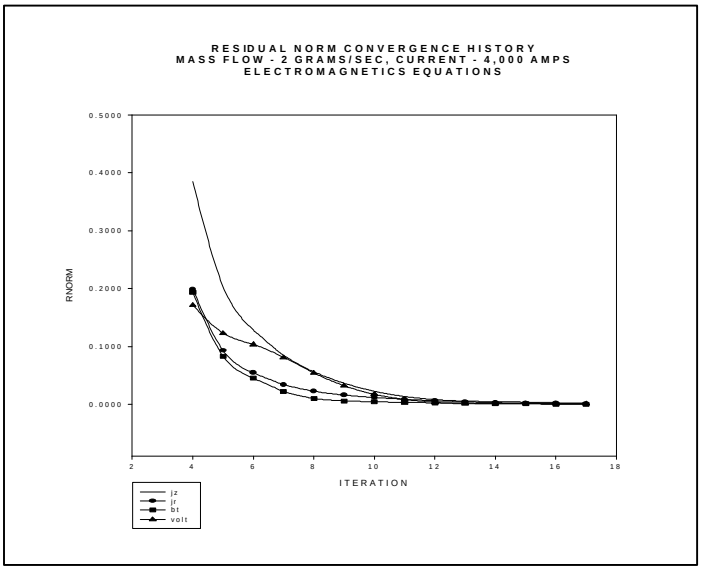


Figure 3. Residual Norm Convergence History – Electromagnetics

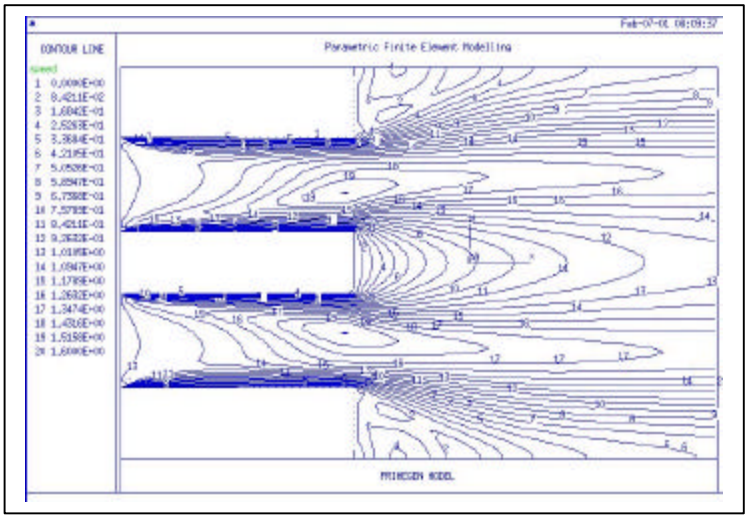


Figure 4. Contour Speed Plot

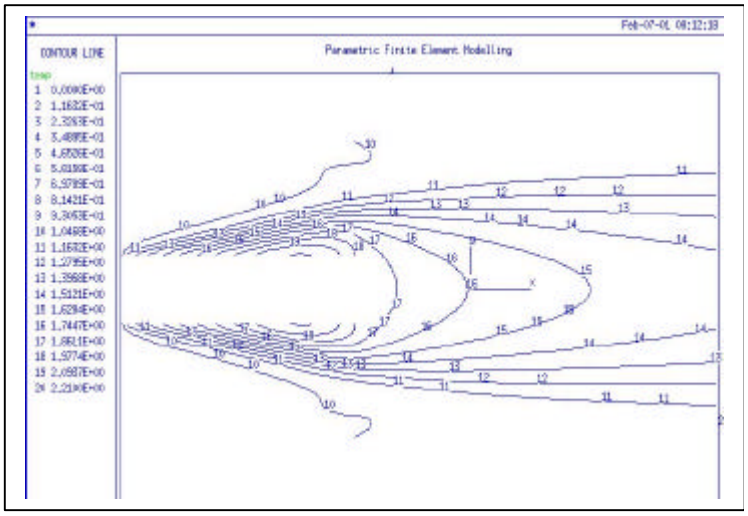


Figure 5. Contour Temperature Plot

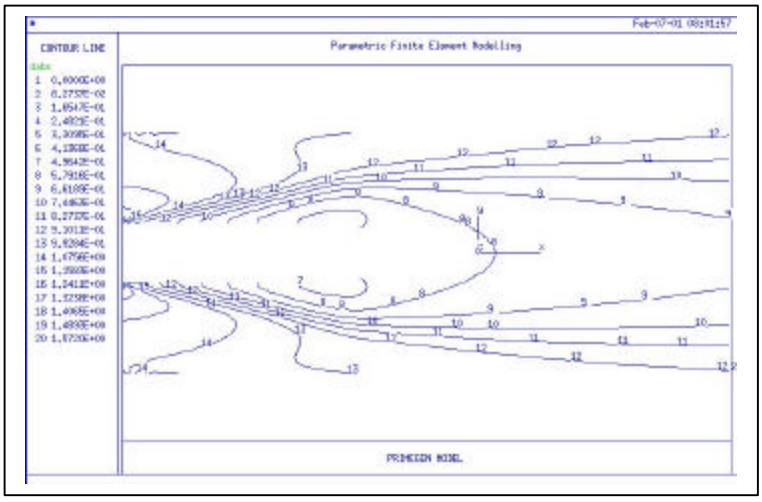


Figure 6. Contour Density Plot

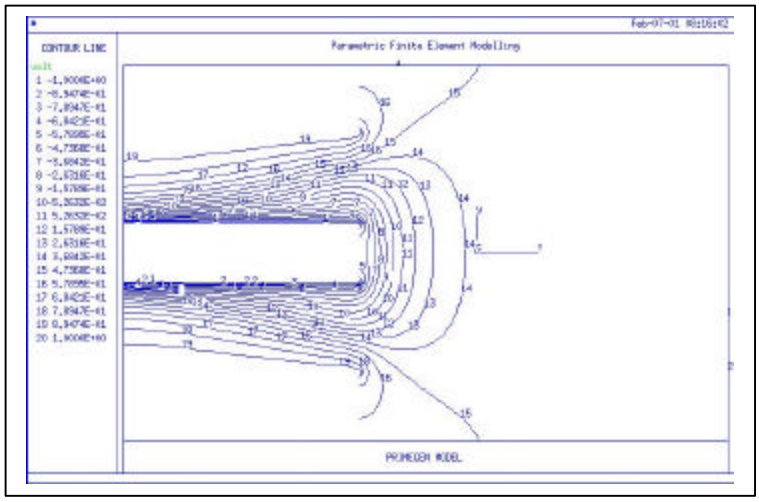


Figure 7. Contour Voltage Plot

## APPENDIX A
## DIMENSIONLESS AND REFERENCE PARAMETERS

Velocity: $V_0 = \dfrac{J_0''^2 X_0}{\Psi_0 s_0 r_0 C_p T_0} \quad m/s$

Mach Number: $Ma = \dfrac{V_0}{\sqrt{g R_{gas} T_0}}$

Pressure: $P_0 = r_0 V_0^2 \quad Pa$

Reynolds Number: $\mathrm{Re} = \dfrac{r_0 V_0 X_0}{m_0}$

Peclect Number: $Pe = \mathrm{Re} \bullet \mathrm{Pr}$

Current Density: $J_0'' = \dfrac{I_0}{2p L_e (R_2 - R_1)} \quad A/m^2$

Voltage: $f_0 = \dfrac{I_0}{s_0} \quad V$

Electric Field: $E_0' = \dfrac{f_0}{L_e} \quad V/m$

Magnetic Flux: $B_0'' = X_0 J_0 m_0 \quad Webers/m^2$

Input Energy Flux: $Q_0'' = c_p T_0 r_0 V_0 \quad W/m^2$

Dissipation Ratio: $\Phi_0 = \dfrac{m_{f_0} V_0^2}{X_0 Q_0''}$

Magnetic Force Ratio: $\Delta_0 = \dfrac{J_0'' B_0'' X_0}{r_0 V_0^2}$

Flow Energy Ratio: $\Pi_0 = \dfrac{V_0 P_0}{Q_0''}$

## APPENDIX B
## LEAST SQUARES [A] MATRIX

$$[A = (N_i)] = \begin{bmatrix} & J_z & J_r & B_q & f \\ 1 & 1 & \dfrac{H B_q}{b_l} & -s\ K_2 v_r & 0 \\ 2 & -\dfrac{H B_q}{b_l} & 1 & s\ K_2 v_z & 0 \\ 3 & \dfrac{\partial}{K_1 \partial r}\left(\dfrac{1}{s}\right) & -\dfrac{\partial}{K_1 \partial z}\left(\dfrac{1}{s}\right) & -\dfrac{K_2}{K_1}\left(\dfrac{\partial v_z}{\partial z} + \dfrac{\partial v_r}{\partial r}\right) & 0 \\ 4 & 0 & 0 & 0 & 0 \\ 5 & 1 & 0 & -\dfrac{1}{r} & 0 \\ 6 & 0 & 1 & 0 & 0 \end{bmatrix}$$

$$\left[A_1 = \frac{\partial (N_i)}{\partial z}\right] = \begin{bmatrix} & J_z & J_r & B_q & f \\ 1 & 0 & 0 & 0 & K_1 s \\ 2 & 0 & 0 & 0 & 0 \\ 3 & -\dfrac{1}{K_1 s} & 0 & \dfrac{H J_z}{b_l s} - \dfrac{K_2}{K_1} v_z & 0 \\ 4 & 1 & 0 & 0 & 0 \\ 5 & 0 & 0 & 0 & 0 \\ 6 & 0 & 0 & 1 & 0 \end{bmatrix}$$

$$\left[A_2 = \frac{\partial (N_i)}{\partial r}\right] = \begin{bmatrix} & J_z & J_r & B_q & f \\ 1 & 0 & 0 & 0 & 0 \\ 2 & 0 & 0 & 0 & K_1 s \\ 3 & 0 & -\dfrac{1}{K_1 s} & \dfrac{H J_z}{b_l s} - \dfrac{K_2}{K_1} v_r & 0 \\ 4 & 0 & 1 & 0 & 0 \\ 5 & 0 & 0 & 1 & 0 \\ 6 & 0 & 0 & 0 & 0 \end{bmatrix}$$